OPEN ACCESS

Marine Sciences ARTICLE

The Innovation Geoscience

In situ observations of methane dynamics in an active cold seep of the Formosa Ridge, the South China Sea

Lei Cao,[1] Chao Lian,[1] Xiangbin Ran,[2] Huan Zhang,[1] Hao Wang,[1] Li Zhou,[1] Hao Chen,[1] Zhaoshan Zhong,[1] Minxiao Wang,[1,3,*] and Chaolun Li[1,4,5,6,*]

*Correspondence: wmx@qdio.ac.cn (M.W.); lcl@qdio.ac.cn (C.L.)

Received: April 16, 2025; Accepted: December 23, 2025; Published Online: January 1, 2026; https://doi.org/10.59717/j.xinn-geo.2026.100192

GRAPHICAL ABSTRACT

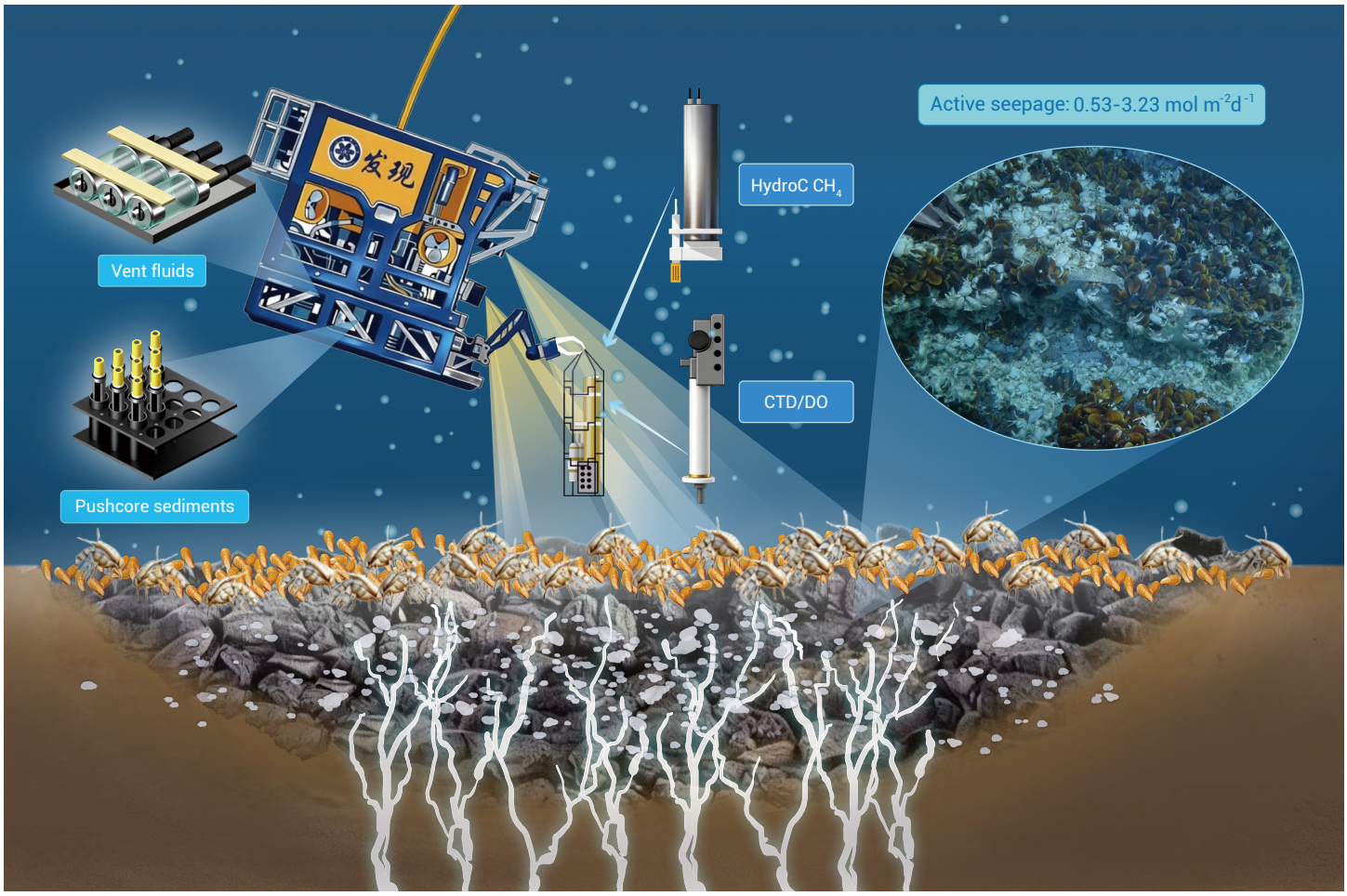

PUBLIC SUMMARY

- Methane released by cold seep profoundly affects the marine environment and contributes to climate change.
- *In situ* observations coupled with steady-state model are employed to quantify methane fluxes from cold seep.
- Horizontal advection is the primary migration mechanism for released methane in the active cold seep.
- The contribution of methane from deep sea cold seeps to the global methane budget have been underestimated.

ARTICLE Marine Sciences

OPEN ACCESS

In situ observations of methane dynamics in an active cold seep of the Formosa Ridge, the South China Sea

Lei Cao,[1] Chao Lian,[1] Xiangbin Ran,[2] Huan Zhang,[1] Hao Wang,[1] Li Zhou,[1] Hao Chen,[1] Zhaoshan Zhong,[1] Minxiao Wang,[1,3,*] and Chaolun Li[1,4,5,6,*]

[1]Center of Deep Sea Research, Institute of Oceanology, Chinese Academy of Sciences, Qingdao 266071, China

[2]Marine Ecology Research Center, First Institute of Oceanography, Ministry of Natural Resources, Qingdao 266061, China

[3]Key Laboratory of Marine Ecology and Environmental Sciences, Institute of Oceanology, Chinese Academy of Sciences, Qingdao 266071, China

[4]Laoshan Laboratory, Qingdao 266237, China

[5]South China Sea Institute of Oceanology, Chinese Academy of Science, Guangzhou 510320, China

[6]University of Chinese Academy of Sciences, Beijing 101408, China

*Correspondence: wmx@qdio.ac.cn (M.W.); lcl@qdio.ac.cn (C.L.)

Received: April 16, 2025; Accepted: December 23, 2025; Published Online: January 1, 2026; https://doi.org/10.59717/j.xinn-geo.2026.100192

Citation: Cao L., Lian C., Ran X., et al. (2026). *In situ* observations of methane dynamics in an active cold seep of the Formosa Ridge, the South China Sea. *The Innovation Geoscience* **4**:100192.

Methane eruptions from active cold seeps profoundly impacts the marine environment and contributes to climate change. However, *in situ* measurements available to constrain the efflux of methane from active seeps are scarce. In this study, *in situ* observations coupled with steady-state model were initially used to evaluate the flux and fate of methane released into the hydrosphere at the cold seep site F. Findings from three years of data indicated that horizontal advection is the primary migration and removal mechanism for released methane, followed by vertical diffusion and microbial oxidation. Methane flux in the active seepage (0.53-3.23 mol m^{-2} d^{-1}) estimated by the in-situ approach was several orders of magnitude greater than that from the sediment-water interface. This would result in 0.70 - 4.22 Gmol yr^{-1} methane being released into the South China Sea (SCS) continental margins. Methane flux estimated based on the *in situ* observation here was significantly higher than that in the previously studied seeps. The regional methane fluxes from cold seeps in the SCS further suggest that dissolved methane discharge substantially contributes to the oceanic methane budget. Extrapolating the methane flux to active seeps worldwide would result in approximately 126 Tg C emitted into the hydrosphere annually as dissolved methane, indicating that the contribution of methane from deep-sea cold seeps to the global methane budget might have been underestimated. Our study emphasizes the deep-sea cold seeps as a significant methane source to the ocean and provides valuable insights into the quantitative assessment of the oceanic methane budget.

INTRODUCTION

The release of methane-rich fluids from subsurface reservoirs to the seafloor frequently occurs along both active and passive continental margins, resulting in the formation of cold seeps.[1,2] Cold seeps are identified as major sources of methane release into the ocean.[3,4] Therefore, studying the transport and consumption processes is essential for understanding the global oceanic methane budget. Extensive studies of cold seeps have shown that they are heterogeneous ecosystems, exhibiting variations in fluid flow intensity and benthic biogeochemical activity.[5,6] Investigating multiple seep systems and conducting numerous measurement iterations are crucial for establishing a well-defined methane budget.

Cold seeps, especially active seeps, have become important areas for studying underwater methane release. Cold seep monitoring primarily relies on underwater sensors, long-term observation and deep-sea sampling equipment to monitor environmental parameters such as temperature, dissolved oxygen (DO) and methane concentration. Monitoring technologies have continuously developed, particularly in multi-beam acoustics and video imaging monitoring. Recent advancements in the quantification of gas emissions at cold seeps have been facilitated by ground-truthing observations from submersibles and remotely operated vehicles (ROVs).[7,8] A key limitation in understanding the role of methane reservoirs at cold seeps in global carbon cycles and climate change is the insufficient attempts to extrapolate individual observations to larger spatial scales. The need for additional *in situ* investigations is evident to validate and enhance existing models, enabling a more comprehensive understanding of the fate of methane released from cold seeps into the ocean. Emerging techniques such as spectroscopic analysis, infrared imaging, and multi-beam acoustic technology have been widely applied in methane measurement. Previous surveys typically employed multi-beam acoustics to monitor gas bubble plumes released from active cold seep vents, or used videos and photos to estimate the size and release rate of bubbles, combined with modeling techniques to calculate the methane release flux.[9,10] However, these methods have long faced challenges in directly and accurately quantifying critical parameters (e.g., bubble size characteristics, acoustic plume distribution, *in situ* methane concentration), often yielding only semi-quantitative or biased estimates. To date, methane discharge flux estimations from deep-water seeps remain scarce, primarily due to their limited accessibility. As a result, data from *in situ* observations have played a pivotal role in emphasizing the importance of cold seeps in the oceanic methane budget. *In situ* observation of the magnitude of methane migrating through the seabed and being released into the hydrosphere and atmosphere continues to pose a key challenge. Furthermore, the widespread occurrence of cold seeps along continental margins highlights the need to characterize their effects on the overlying water.[11] *In situ* exploration of the environmental conditions of deep-sea cold seeps could advance our understanding of the biogeochemical processes occurring in the water column above seafloor seepage sites.[6,12,13]

The northeastern slope of the South China Sea (SCS) hosts the most active gas seepage at site F, which sustains a highly productive chemosynthetic ecosystem.[14,15] However, the quantification of methane flux from this active seep into the hydrosphere in this region is currently limited. This restriction hampers our understanding of its connections with adjacent ecosystems and affects our evaluation of the cold seep systems' contribution to the oceanic methane budget. In this study, an *in situ* multi-sensor system was deployed to explore the environmental characteristics of the water column above various seafloor habitats at site F in 2017, 2018, and 2020. Using the findings from the *in situ* observations, a steady-state box model was employed for the first time in SCS to assess the flux and fate of methane emitted from the seabed into the hydrosphere at site F. Additionally, a comparison was made between the methane flux at the sediment-water interface and across different cold seep habitats to enhance our understanding of the methane budget. The primary aim of this research is to estimate methane emission flux from the deep-sea cold seep using *in situ* data and to improve our understanding of the sources, transport mechanisms, and fate of methane in the marine environment.

MATERIALS AND METHODS

Geological setting

The Formosa Ridge lies along the northern continental margin of the South China Sea, offshore of southwestern Taiwan. The cold seep under investigation, referred to as site F (Figure S1), is located on the slope ridge of Formosa Ridge (119°17'08.287, 22°06'55.425), which spans approximately 30 km in length and 5 km in width.[14,16] Its flanks are steep, with a maximum slope angle exceeding 30 degrees, and two summits, separated by 2 km, have formed on the Formosa Ridge.[17] The eastern part of the ridge marks the deformation front where the Luzon subduction system intrudes upon the SCS continental margin.[16] The water depth at the southern summit, where the

active cold seep is located, is approximately 1125 m.[18] As an active gas seepage site on the northeastern slope of the SCS, site F exhibits a highly heterogeneous seafloor habitat and productive chemosynthetic ecosystems.[15,19,20] These traits, which span habitat structural complexity and ecosystem functional output, may reflect universality across global cold seep systems.

The cold seep vent has been explored using the Jiaolong manned deep submersible and the ROV Faxian during multiple research expeditions.[21,22] Detailed mapping, multichannel seismic analysis, and *in situ* observations of the cold seep area have been conducted.[13,22,23] Site F has acted as a natural laboratory for studying biogeochemical processes, the evolution of the cold seep system, and fluid sources.[16,24,25] The seismic profile reveals a distinct, continuous bottom simulating reflection (BSR) underlying the ridge and a clear vertical migration pathway from the deeper subsurface to the seafloor.[16] BSR is an acoustic impedance contrast between gas hydrate-bearing sediments and underlying free gas layers, formed by the vertical migration of methane and other gases. Gases rising along faults to the hydrate stability zone form hydrate caps, with the remaining gas accumulating below, creating a high-amplitude, negative-polarity reflection. Fluctuations in BSR depth can indicate changes in deep fluid flux. Large and dense benthic chemosynthetic communities primarily consist of dense populations of bathymodiolid mussels (*Gigantidas platifrons*) and galatheid crabs (*Shinkaia crosnieri*) (Figure 1; captured *in situ* with a camera on the ROV Faxian). Furthermore, extensive authigenic carbonates and distinct gas flares have been observed at this highly active seepage site.

In situ detection of the water column environment around the cold seep

The multi-sensor system used for *in situ* environmental detection consisted of several integrated sensors (Figures 1G-I). These components were assembled and integrated into an articulated frame. The primary components included the CONTROS HydroC CH_4 sensor (Kongsberg Gruppen, Norway), Seabird SBE 25 Plus conductivity-temperature-depth (CTD) sensor (SeaBird, USA), and Seabird SBE37 sensor (SeaBird, USA). The detector of the CONTROS HydroC CH_4 sensor is a high-precision optical analysing NDIR (Non-Dispersive Infrared, NDIR) system. Dissolved methane diffuses from the liquid through a patented thin film composite membrane into an internal gas circuit. Therein the concentrations are measured by non-dispersive infrared spectrometry. The sensors measure in real time and store data to an internal data logger at different operating water depths (Table S1). Every HydroC™ CH_4 sensor used to the underwater exploration has been calibrated individually and *in situ* within a special insulated water tank. Due to its small size and weight (2.6 kg in water) an integration of the instrument into various static as well as moving platforms can be easily achieved. The composition of the multi-parameter sensors was presented in the supplementary information (Figure S2). This integrated device was deployed on the tool sled in front of the ROV Faxian and subsequently held by a manipulator arm to approach various sites for detailed *in situ* detection. Based on previous surveys of the seafloor habitats in the study area, the multi-sensor system was extensively deployed over the cold seep.

This system covered the active vent, associated chemosynthetic communities, carbonate patches, and surrounding sediments to collect data on the distribution and variations of environmental parameters in the overlying water of the cold seep. The environmental conditions of the cold seep were recorded through *in situ* detection along the entire ROV tracks. The concentrations of dissolved methane and oxygen were obtained with error ranges of ± 3% and ± 0.1%, respectively. During *in situ* detection, the multi-sensor system platform was held by the ROV's manipulator arm and positioned at the seabed surface until the output data from the sensors at the specific site stabilized. The deviation between two consecutive measurements should not exceed ±3%. The multi-sensor system aboard the ROV Faxian was used to conduct seafloor *in situ* observations during three cruises in 2017, 2018, and 2020. These surveys were planned and conducted in a controlled manner to ensure complete coverage of specific areas in the cold seep and to obtain sufficient measurement repetition. In addition, a current meter was fixed to the device on the seafloor near the active cold seep to measure the near-seabed velocity of the bottom current in this region (Aquadopp 6000 m Nortek, Norway) with an accuracy of ± 1%.

Sample collection

During the Kexue cruises in 2017, 2018, and 2020, the ROV Faxian was used to perform seafloor observations and sampling in the study area surrounding the active cold seep. Discrete samples were collected using a multi-sampler operated by the ROV Faxian. Fluids were collected in 150 mL gas-tight samplers to recover both liquid and gaseous samples from the cold seep vent. Additionally, water samples from around the vent were collected using 5-liter Niskin bottles attached to the rear of the ROV. In this study, we used a 0.7 μm glass fiber filter membrane to filter seawater samples for dissolved inorganic carbon (DIC) and dissolved organic carbon (DOC) measurements. The fiber glass membranes have been calcined at 450°C and then cleaned with deionized water. Push cores were collected from various sites of the cold seep by the ROV. After retrieval of the push cores on deck, 3 mL of sediment was transferred with a 5 mL cut-off syringe into a 22 mL serum vial containing 3 mL of 2 mol L^{-1} NaOH. The vial was crimp-sealed and stored at 4°C for sediment methane analysis. Porewater was extracted at 2 cm depth intervals using Rhizon samplers with a 0.2 μm pore size (Rhizosphere, The Netherlands). After recovery of the samplers onboard, the fluids in the gas-tight bottles were promptly transferred to gas sampling bags for gas component extraction.

Analyses

Methane concentrations were measured using a gas chromatograph equipped with a flame ionization detector (Agilent 7890, USA). The carbon isotope ratios of CH_4 in the vent fluids and sediments were determined using continuous-flow isotope ratio mass spectrometry (IRMS) (Trace GC Ultra/Delta V Advantage, Thermo Scientific, USA), with analytical errors of approximately 0.5‰. The stable carbon isotope ratios were expressed in the standard notation on the per mil scale relative to Vienna-PDB. Once the ROV was back on board, the fluid samples were processed. The pH of the fluids was measured onboard immediately after the ROV was recovered. Hydrogen sulfide in the fluids was measured using the methylene blue method, with an error margin of ± 3%. Dissolved organic carbon (DOC) concentrations were measured using a high-temperature catalytic combustion method on a total organic carbon analyzer (TOC-V CPH, Shimadzu, Japan), with an analytical precision of 3%. $\delta^{13}C_{DOC}$ was analyzed using an Isoprime 100 continuous flow isotope ratio mass spectrometer, with an analytical precision better than 0.3‰. DIC and $\delta^{13}C_{DIC}$ were determined using a Thermo Finnigan Gas Bench coupled with a MAT 253 IRMS (Thermo Scientific, USA) with an analytical precision better than 0.2‰. Nutrients (NO_3^-, NO_2^-, NH_4^+, SiO_3^{2-}, PO_4^{3-}) concentrations in the fluids were determined using a QuAAtro continuous flow analyzer (SEAL Analytical GmbH, Germany), with an analytical precision of 5%. Sulfate concentrations were measured using a Dionex Ion Chromatograph (Thermo Scientific Dionex, USA), with an analytical precision better than 2%.

Flux modeling

The modeling approach employed here is based on a geochemical box model and previous steady-state models of seawater CH_4 concentration.[26,27] In the model, the concentration of dissolved CH_4 in the water column was assumed to be in a steady state. Therefore, the source of CH_4 entering this region could be determined based on the amount necessary to balance the sum of CH_4 losses. The feasibility of the steady-state assumption in this region was confirmed by comparing the *in situ* methane concentrations of the cold seep measured in 2017, 2018 and 2020. It is reasonable because there is no significant change in the magnitude or morphology of the water column CH_4 distributions above the cold seep. Detailed input parameters of the box model are presented in Table S2.

The study region in the cold seep is represented in this model as a simplified box (Figure 2). This model constrains CH_4 losses from the box via vertical diffusion (*Dif*), horizontal advection (*Adv*) including the zonal velocity and the meridional velocity as shown in Figure 2, and biological oxidation (*Ox*), each with units of mol d^{-1} (equation (1)). The input of CH_4 (mol d^{-1}) into the box could be determined as the sum of the loss terms (*Dif*, *Adv*, and Ox) for the box. The methane flux (mol m^{-2} d^{-1}) or volume input rate (mol L^{-1} d^{-1}) can be obtained by dividing the input by the area or volume of the box, respectively. The influence of advection on CH_4 concentrations was also considered as follows:

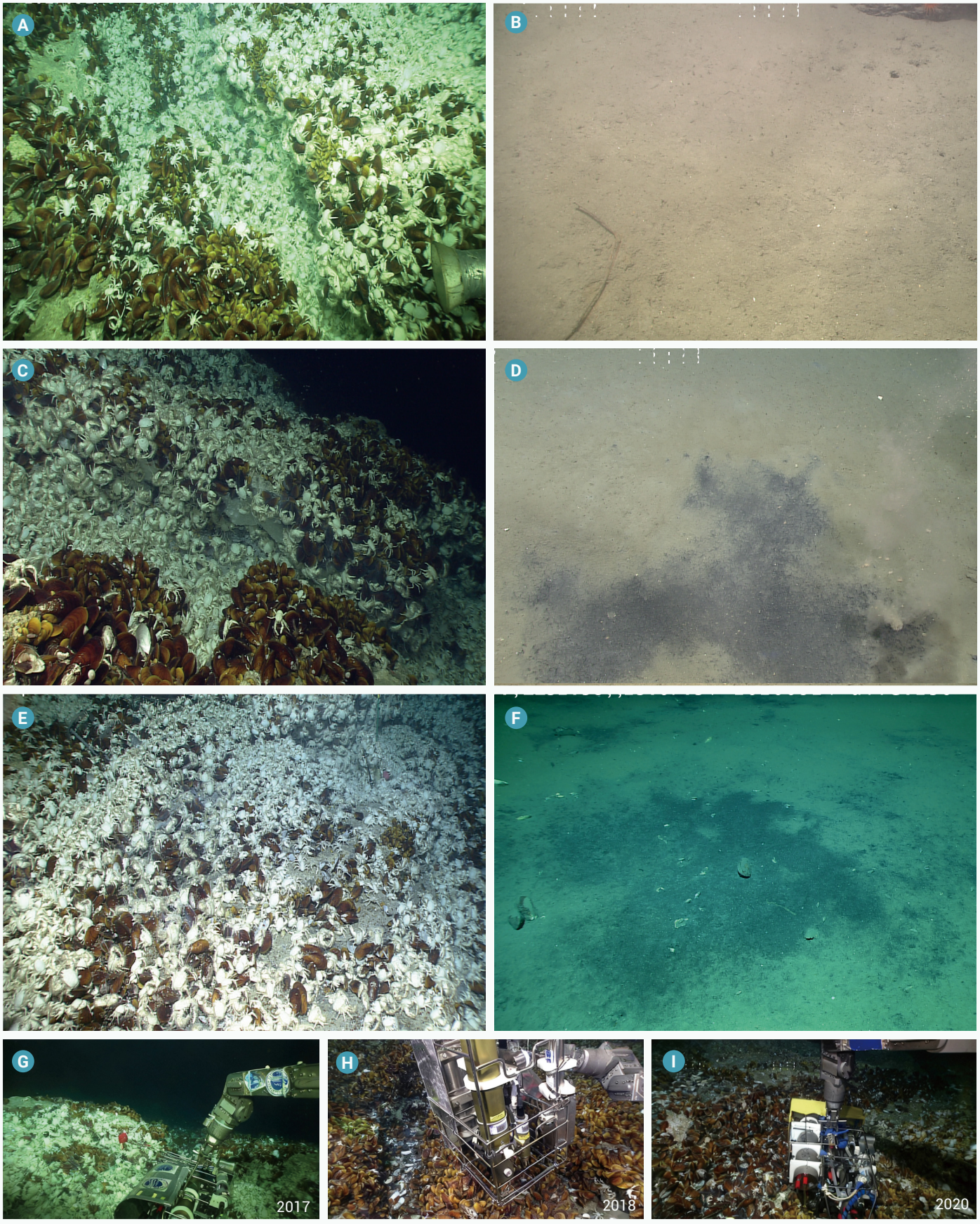

Figure 1. Images of different seafloor habitats and *in situ* detection of the cold seep during three years (A, C, E) The active seepage area with dense benthic communities covered in 2017, 2018 and 2020. (B) Background sediments. (D, F) Reduced sediments. (G-I) Multi-sensor system for *in situ* detection of the cold seep during three years.

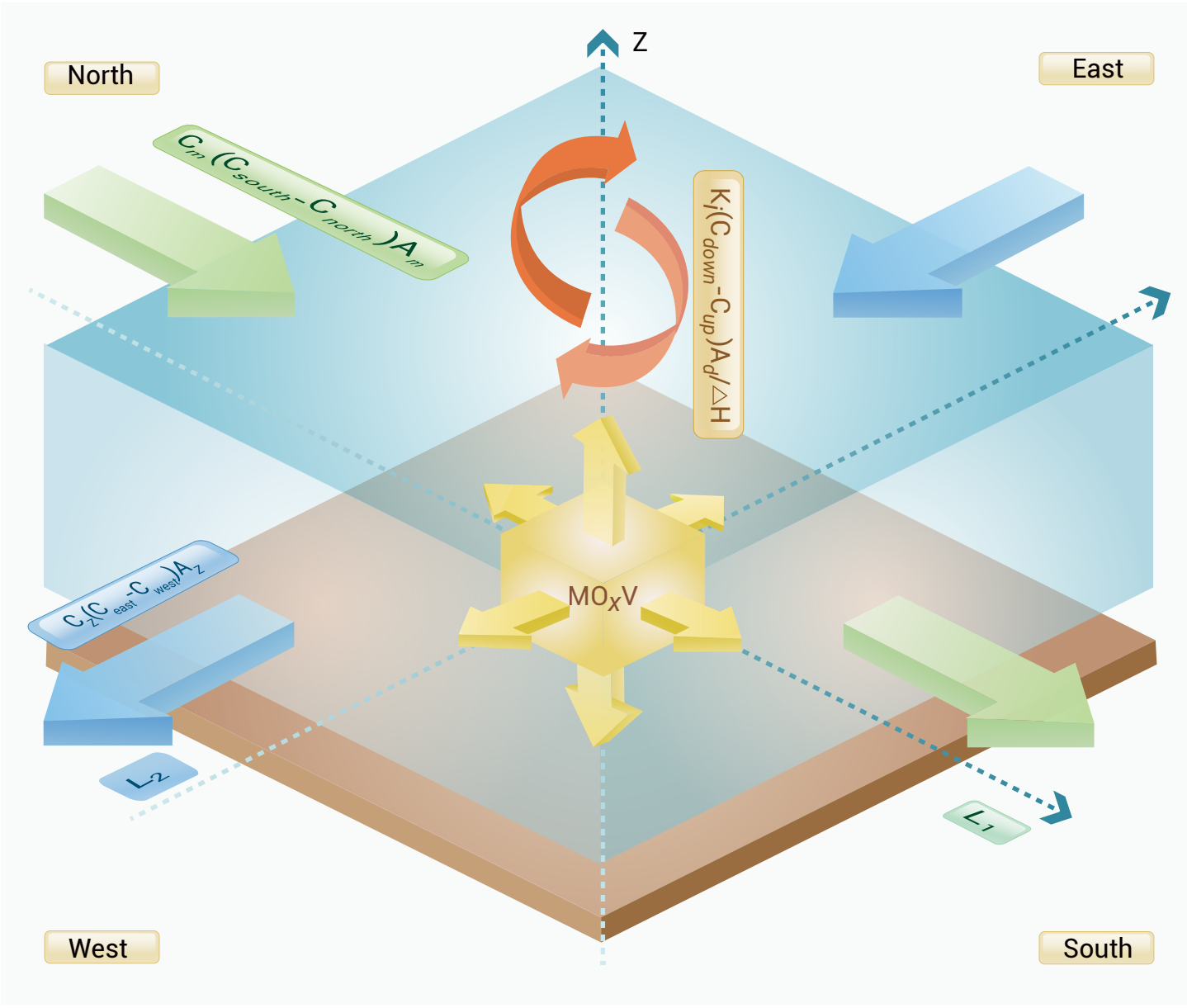

Figure 2. Illustration of the geochemical box model including the sinks of CH_4.

$$\frac{dCH_4}{dt} = Sources - Dif - Adv - Ox = 0 \quad (1)$$

Where, vertical diffusion was modeled following Fick's first law of diffusion and was constrained at the top of the box (Figure 2):

$$Dif = \frac{K_i A_d (C_{down} - C_{up})}{\Delta H} \quad (2)$$

Where, K_i is the diffusion coefficient (m^{-2} d^{-1}), andΔH (m) is the height of the box. C_{down} and C_{up} represent the concentration of dissolved CH_4, and A_d(m^2) is the cross-sectional area of the top of the box. Values for K_i are chosen based on observations in the surrounding region.[28] Additionally, a sensitivity study of the K_i values for the input methane fluxes is conducted below.

Horizontal advective additions and losses of CH_4 are calculated using:

$$Adv = C_{sz}(C_{east} - C_{west})A_z + C_{sm}(C_{south} - C_{north})A_m \quad (3)$$

Where, C_{sz} and C_{sm} (m^{-2} d^{-1}) represent the zonal velocity and meridional velocity of water currents moving through the region. A_z represents the zonal cross-sectional area, and A_m represented the meridional cross-sectional area. C_{east}, C_{west}, C_{south} and C_{north} are the average concentration of dissolved CH_4 at the edges in different directions. The current speed and direction are determined through *in situ* observation from the current meter deployed on the seafloor of the cold seep during our cruise, and current direction is used to define the region that is upstream.

Methane oxidation is calculated as follows:

$$Ox = MOxV \quad (4)$$

Where, *MOx* is the methane oxidation rate in the box in units of μmol $L^{-1}d^{-1}$. *V* is the volume of the box. The value of *MOx* is chosen based on values in previous studies in the vicinity of the study area according to the measured dissolved CH_4 concentration in the bottom water.[29] Due to the highly variability of *MOx*, a sensitivity study of the values of *MOx* for the input methane fluxes is also conducted and discussed below.

Diffusive fluxes (*J*, μmol cm^{-2} yr^{-1}) of dissolved methane (*C*, μmol L^{-3}) in the sediments are calculated using Fick's First Law:

$$J = \phi \times D_s \times (dC/dz) \quad (5)$$

Where, *z* is the depth (cm), D_s is the diffusion coefficient of bulk sediment in cm^{-2} yr^{-1}, which is derived from the porosity (φ) and molecular diffusion coefficients in free solutions of seawater at 4°C ($D_{sw\text{-}CH4}$ = 8.97 × 10^{-6} cm^2 s^{-1}),[30] as previously explained ($D_s = D_{sw} / (1 + 3[1-\varphi])$,[31] and the *dC/dz* is the linear gradient of the concentration profile.

Table 1. Physicochemical characteristics of the fluids from the active seepage.

Environmental variable (Units)	Value range	Sample/Parameter obtained
Temperature (°C)	3.59-3.63	*In situ*
Salinity	34.55-34.63	*In situ*
DO (mg/L)	2.91 - 3.21	*In situ*
CH_4 (μM)	7-55	*In situ*
$\delta^{13}C_{CH4}$ (‰)	−68.50- −71.20	Gas-tight sampler
pH	7.70-7.87	Gas-tight sampler
H_2S (μM)	0-35	Gas-tight sampler
DIC (mM)	1.93-2.30	Gas-tight sampler
$\delta^{13}C_{DIC}$ (‰)	−2.43- −3.40	Gas-tight sampler
DOC (μM)	155-211	ROV-$_{CTD}$
$\delta^{13}C_{DOC}$ (‰)	−25.16- −27.30	ROV-$_{CTD}$
SO_4^{2-} (mM)	28.03-28.29	ROV-$_{CTD}$
NO_3^- (μM)	21.72-22.93	ROV-$_{CTD}$
NH_4^+ (μM)	2.16-4.12	ROV-$_{CTD}$
NO_2^- (μM)	0.33-0.40	ROV-$_{CTD}$
SiO_3^{2-} (μM)	84-100	ROV-$_{CTD}$
PO_4^{3-} (μM)	1.80-1.96	ROV-$_{CTD}$

RESULTS

Venting fluids from the active seepage

We summarized the environmental variables of seep fluids collected above the active vent by ROV during cruises at site F from 2017 to 2020 (Table 1). The *in situ* measurements of oxygen concentrations ranged from 2.91 to 3.21 mg L^{-1}, indicating a hypoxic environment (a DO threshold of 3.20 mg L^{-1}) in the vicinity of the vent.[32] The *in situ* salinity ranged slightly from 34.55 to 34.63, while the temperature varied between 3.59°C and 3.63°C. Methane concentrations were also measured *in situ*, ranging from 7 to 55 μM. The pH of the venting fluids ranged from 7.70 to 7.87. Hydrogen sulfide concentrations in most samples were below the detection limit, with the highest hydrogen sulfide concentration in vent fluids being 35 μM. The DIC concentration ranged from 1.93 to 2.30 mM, showing a slight negative drift (-2.43 −3.40 ‰) in $\delta^{13}C_{DIC}$ relative to open seawater. The DOC concentration ranged from 155 to 211 μM, and $\delta^{13}C_{DOC}$ varied from -25.16 ‰ to -27.30 ‰. The sulfate concentration and abundant nutrients in the vent fluids showed no significant fluctuation, suggesting a relatively stable geochemical environment and an adequate nutrient supply.

In situ measurement of the overlying water above the seafloor of the cold seep

Based on real-time synchronous observation data collected during three cruises (Figure 3), the fluctuations in DO, temperature, and salinity were closely linked to variations in methane concentration (Figures S4-S6). Elevated methane concentrations in the bottom water corresponded to active seepage sites, characterized by a dramatic drop in DO levels (Figure S7, R^2 = 0.994, $p < 0.05$). This correlation was particularly evident in areas rich in chemosynthetic communities (Figure S3). Simultaneously, the most noticeable fluctuations in bottom water temperature were also associated with increased methane concentrations (Figure S5). The elevated temperature were often accompanied by higher methane concentration (R^2 = 0.515, $p < 0.05$), especially in 2017. We also observed that salinity in the bottom water significantly decreased as methane concentrations increased. Furthermore, the distribution of DO, temperature, and salinity indicate that impact of methane emissions on the physicochemical environment of the adjacent water column (Figure 4).

During the three cruises, the seabed features and *in situ* environmental detection results of biological coverage revealed a relatively stable pattern of methane eruption at the cold seep (Figure 1). Although short-term concentration changes could occur, the methane concentration at the center of the active seepage remained generally stable over annual timescales. Specifically, methane concentration showed significant spatial variation across the cold seep. The highest concentration was recorded at the active seepage site, where dense chemosynthetic communities thrived (Figure S7). Generally, methane concentration decreased with increasing distance from the venting site. The highest methane concentration measured at the active vent during the three cruises ranged from 6.87 to 55.9 μM. At the outermost area, where sediments were covered, methane concentration was much lower. In contrast, DO concentration increased with distance from the venting site, and the lowest DO levels were observed at the site with the highest methane concentration. The bottom water temperature at the active seepage site appeared slightly higher than that of the surrounding seawater, while its salinity was relatively low.

Methane emission and flux of the active seep

The results of the steady-state box model quantified the input of methane and its flux in the cold seep, as shown in Table 2. These estimates, based on *in situ* detection at the cold seep, were extrapolated to the entire extent of Site F to provide constraints on the overall emission budget and methane release rate in this area.

The sensitivity of the model was tested by both increasing and decreasing horizontal current velocity (C_z, C_m) and vertical diffusion coefficient (K_i) by a factor of 2, and the methane oxidation rate (*MOx*) by factors of 2 and 10 for recalculating the seep methane emissions over three years. Meanwhile, the methane oxidation rate was highly variable in both space and time. Therefore, an additional factor of 10 was included in the sensitivity test of the model. As shown in Table 2, the predicted range of the seep methane inputs and flux was obtained by simultaneously increasing or decreasing all the model parameters by the factors mentioned above. The model predicted a minimum seep methane flux of 0.26 mol m^{-2} d^{-1} in 2018 and a maximum of 6.61 mol m^{-2} d^{-1} in 2020. In 2017, the seep methane flux ranged from 0.97 to 4.07 mol m^{-2} d^{-1}. In summary, the total seep methane emission ranged from 1.96 to 50.2 Mg CH_4 yr^{-1} based on the sensitivity test results over the three years, whereas the base estimates were between 4.04 and 24.5 Mg CH_4 yr^{-1}. These experiments account for natural variations in measurements, which may be influenced by changes in the conversion efficiency of methane. When methane was transformed in the environment, it can be converted into biomass or dissolved inorganic carbon, which reduced the methane concentration that was measured in the field. In the sensitivity tests, the impact of methane conversion efficiency was further amplified by adjusting parameters such as horizontal flow velocity, vertical diffusion coefficient, and methane oxidation rate. Therefore, the conversion efficiency of methane plays a critical role in both in-situ methane measurements and flux estimates.

Processes of the methane sinking

Since the sensitivity parameters varied based on potential changes that occurred during natural processes, these exercises with different parameter combinations could provide insights into the contribution of various seafloor processes to the methane sink. Across all the cruises, horizontal advection consistently dominated the methane sinking processes (Figure 5A). The average proportion of the horizontal advection term reached 84.8%, followed by vertical diffusion and microbial oxidation of methane. This implied that about 15.2% of seepage methane would be transformed within local waters through two pathways, including rapid oxidation occurring in bottom waters, and upward diffusion through water column with progressive oxidation across different depth layers. Ultimately, this portion of methane may be oxidized to CO_2 or remain in the water column, thereby exerting substantial impacts on the regional carbon cycling dynamics.

We also evaluated the effect of each model parameter on the predicted seep methane flux by individually varying the specific parameter while keeping all other parameters constant (Figure 5B). These sensitivity tests showed that seep methane flux were insensitive to changes in vertical diffusion or microbial oxidation of methane, but were substantially influenced by variations

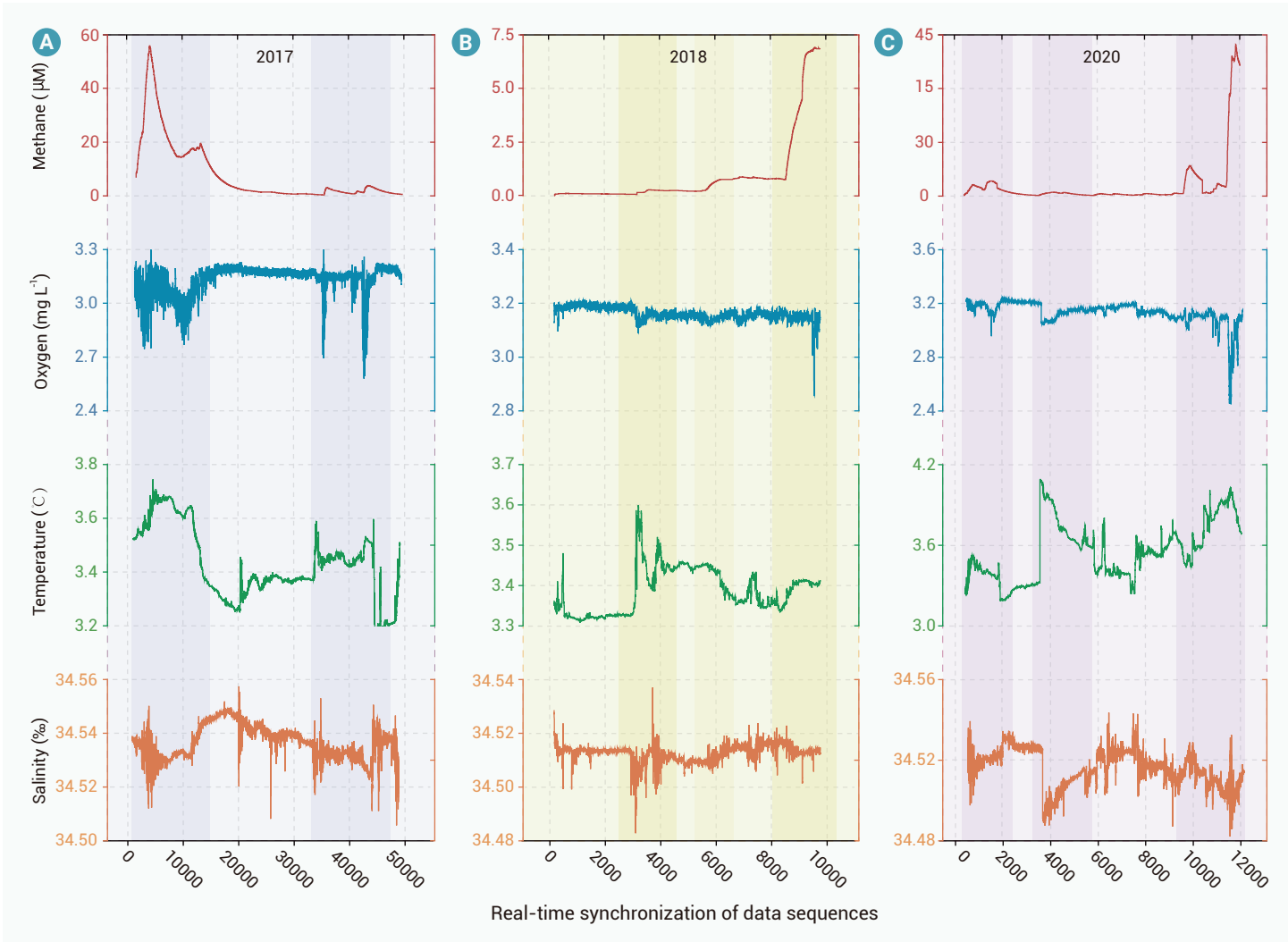

Figure 3. Synchronously acquired environmental parameters through *in situ* measurements across the cold seep (A-C) *In situ* environmental parameters of bottom water obtained in 2017, 2018 and 2020, respectively.

in horizontal advection. Therefore, the model results for all three years indicated that horizontal advection was the primary migration/removal mechanism for the methane released from the subseafloor into the overlying water.

Methane in sediments of the cold seep

In this study, we classified the sediment samples into two groups: methane-rich and background, based on methane concentration and seafloor habitats (Table 3). The sulfate and methane profiles in the pore water of the sediments varied systematically across different habitats in the study area (Figure 6). In methane-rich sediments, CH_4 concentrations increased with depth, while sulfate concentrations decreased sharply. This suggests that anaerobic methane oxidation occurred in the methane-rich, reduced sediments. The maximum CH_4 concentrations in the four methane-rich sediment profiles ranged from 4690 to 8620 μM. The $\delta^{13}C_{CH4}$ values in methane-rich sediments increased with depth. The $\delta^{13}C_{CH4}$ values were highly negative, ranging from -88.31‰ to -78.22‰, indicating a dominant biogenic origin of methane in the shallow sediments of the cold seep.[13,21] In comparison to the methane-rich sediments, methane in the background sediments was relatively low, while the sulfate concentration (27.8-28.9 mM) in the profiles remained nearly constant with depth. As a result, the methane flux was 0.51 μmol m^{-2} d^{-1} in the coral zone sediment, far from the active seepage, and 2.32 μmol m^{-2} d^{-1} in the relatively closer bare sediment, compared to the former site (Table 3). The methane flux varied from 890 to 2500 μmol m^{-2} d^{-1} in the methane-rich sediments across the cold seep sites, including the northern and southern black-reduced sediments around the cold seep.

DISCUSSION

Biogeochemical characteristics of bottom water related to the methane eruption

Oxygen concentration in bottom water is critical for regulating respiration rates at cold seeps. It influenced the reactivity of organic matter, microbial metabolism, and the distribution of fauna.[11,33] According to *in situ* measurements, DO concentration dropped dramatically in the methane-enriched area with dense chemosynthetic communities, indicating enhanced oxygen consumption by methanotrophs, benthic macroorganisms and other oxygen-consuming microorganisms. As the water depth of site F reached the OMZ of the tropical western Pacific Ocean, the overlying water was approaching hypoxic condition.[32,34] Furthermore, the ongoing methane eruption could exacerbate this hypoxia. Due to intense biological activity in active seepage, nutrients in overlying water could turnover rapidly. Although nitrate accumulated in the bottom water of the site F, its concentration was relatively low compared to that in the water column at the same depth in the western Pacific Ocean.[34] The nitrate in the bottom water may have undergone dissimilatory nitrate reduction in the active seepage.[35] The significant negative $\delta^{13}C$ signature of the methane recovered from the venting fluids could lead to products with negative isotopic values. The slight negative drift of $\delta^{13}C_{DIC}$ and $\delta^{13}C_{DOC}$ in the venting fluids, compared to open seawater, also indicated the rapid turnover of methane and its impact on the overlying water (Table 1). Additionally, an increase in methane concentration was observed to coincide with elevated temperatures and decreased salinity of the bottom water. We hypothesize that the heat exchange exist between the released methane and the surrounding water. Water temperature increase may trigger the dissociation of shallow submarine gas hydrates, leading to the release of methane.

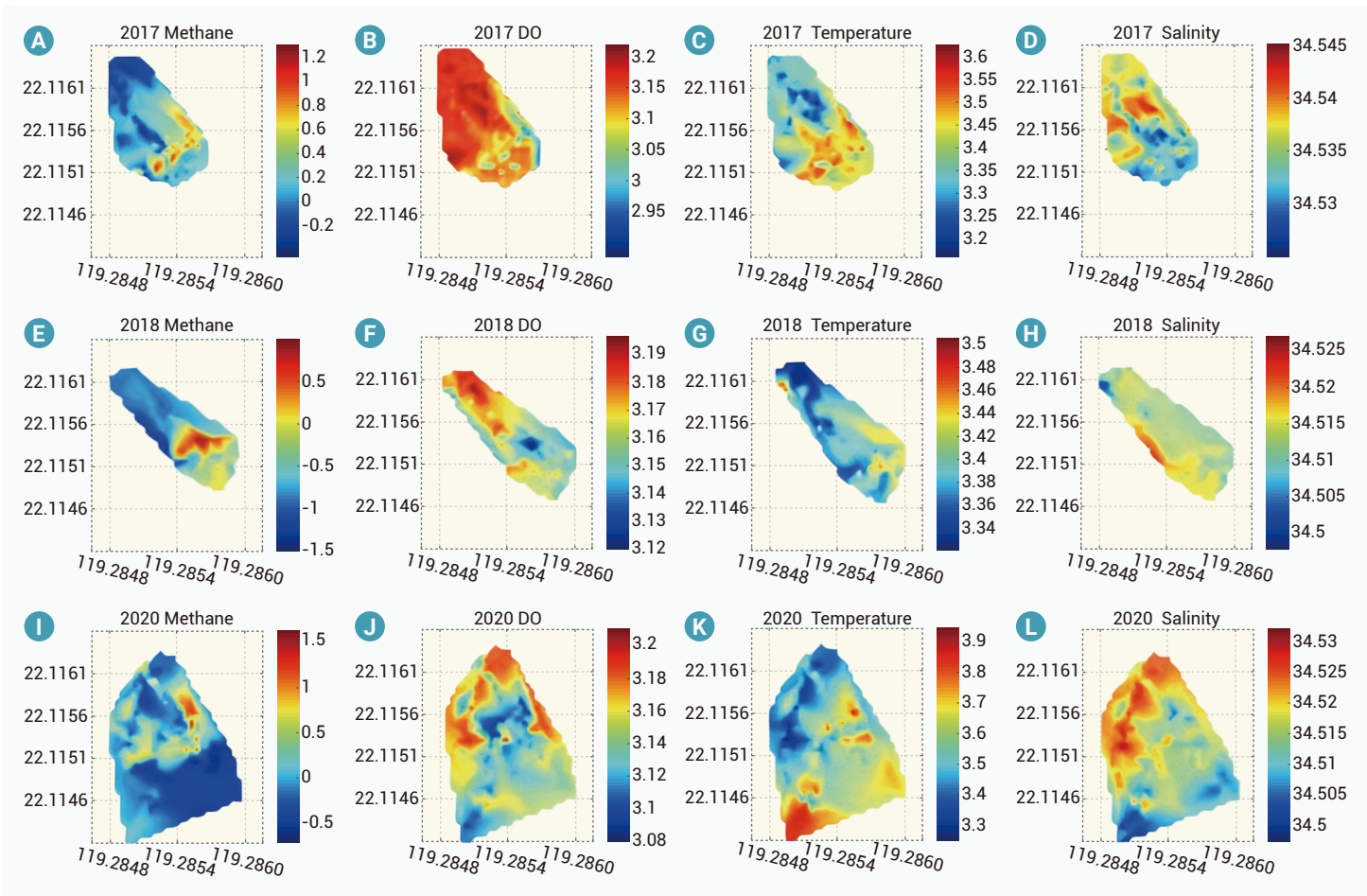

Figure 4. Spatiotemporal variation of environmental parameters in the bottom water of the cold seep (A,E,I) Dissolved methane (μM in logarithmic scale), (B,F,J) DO (mg L^{-1}), (C,G,K) Temperature (°C) and (D,H,L) Salinity (‰).

Table 2. Sensitivity test results of the methane inputs and flux in the cold seep[a].

Sensitivity range	Methane flux (mol m^{-2} d^{-1})			Methane flux (kg L^{-1} d^{-1})			Methane inputs (Mg yr^{-1}, 1M=10^6)		
	2017	2018	2020	2017	2018	2020	2017	2018	2020
Low Estimate	0.97	0.26	1.60	1.55	0.41	2.57	7.36	1.96	12.2
Base Estimate	1.96	0.53	3.23	3.13	0.85	5.16	14.9	4.04	24.5
High Estimate	4.07	1.22	6.61	6.52	1.96	10.6	30.9	9.28	50.2

[a] The low and high values were estimated by decreasing and increasing horizontal current velocity and K_i by factors of 2, with *MOx* by a factor of 10 simultaneously.

Concurrently, the freshwater liberated during hydrate dissociation could cause a local decrease in water salinity. Nevertheless, these potential mechanisms need to be validated through long-term *in situ* observations, such as deploying seafloor observation networks. These results could provide more accurate insights into the impact of venting methane on overlying water in chemosynthetic ecosystems at the active seep.

Spatiotemporal variation of the methane in the hydrosphere of the cold seep

The complex interactions among biological, geochemical, and geological processes have shaped highly diverse habitats on the seafloor. The unique environmental conditions of the hydrosphere in active seep areas provided an opportunity to explore the interactions between chemosynthetic ecosystems and the surrounding benthic ecosystems.[36] Environmental conditions in cold seeps were unstable over short time scales due to temporal fluctuations in the reduced compounds released from the subseafloor. These fluctuations further shaped regional chemical spatial distributions across the seafloor. The site F exhibited distinct substrate features, with authigenic carbonates dominating the central region and muddy sediments prevailing in peripheral areas (Figure 1), likely due to the succession of cold seeps. Most macrofauna were located on or near hard substrates, particularly in areas with evident seepage. These structures, created by authigenic carbonates, enhanced habitat diversity and may serve as migration pathways for seepage. The active seepage vent was located at the central authigenic carbonates, where the dominant species,[37] *Gigantidas platifrons* and *Shinkaia crosnieri*, reached their highest densities of 629 and 396 individuals/m^2, respectively.

According to *in situ* measurements, methane concentrations varied horizontally across the cold seep, showing a decreasing gradient from the central benthic communities to the desert-like area at the edge of the cold seep. Despite the methane eruption causing significant heterogeneity due to the varied environments on the seafloor, high concentrations of dissolved methane and the most intense environmental fluctuations were confined to the center of the active seep site, where dense chemosynthetic communities thrived. Here, the highest biomass densities were achieved by assemblages of chemosynthetic bathymodioline mussels and squat lobsters with intracel-

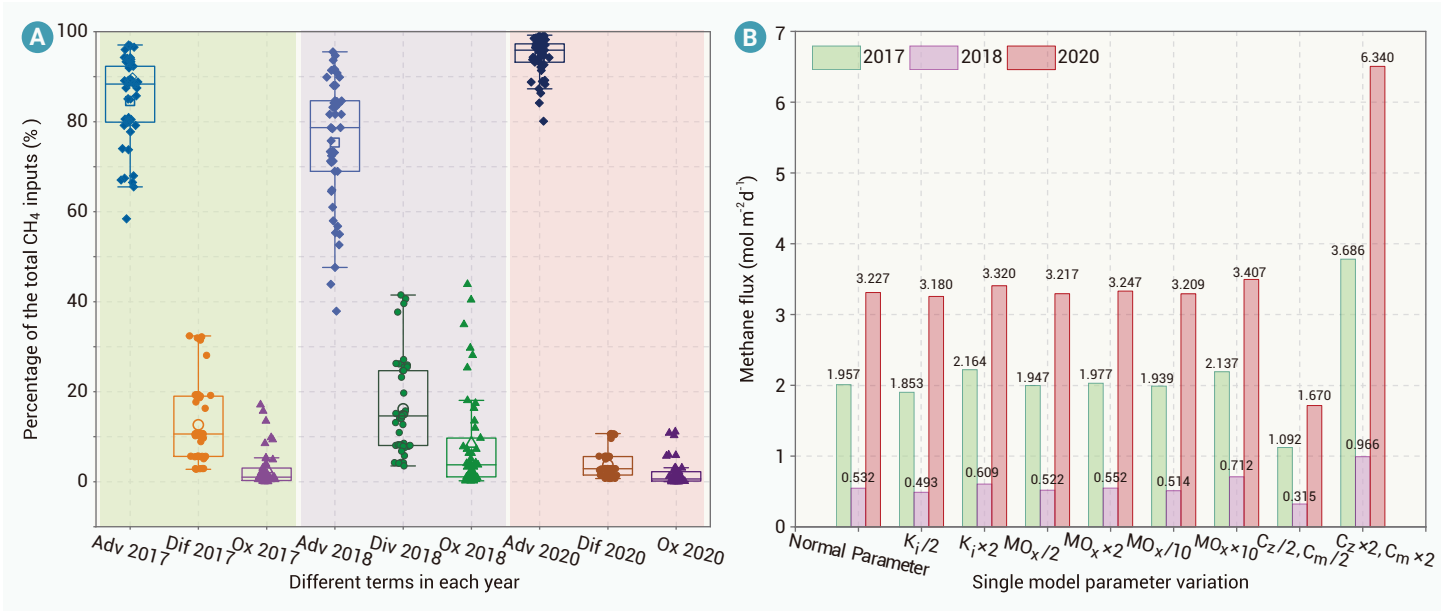

Figure 5. Model results and sensitivity analysis (A) The contribution of each term to the total methane sink. (B) Sensitivity of the methane inputs into the cold seep to modeled parameters.

Table 3. Sampling information and methane fluxes of sediments in the cold seep.

Samples	Water depth (m)	Methane supply	Habitat type	Methane flux (μmol m^{-2} d^{-1})	Methane flux (g m^{-2} yr^{-1})
PC-C	1235	Background	Coral zone sediment	0.51	0.009
PC-B	1165	Background	Bare sediment	2.32	0.04
PC-MN1	1148	Methane-rich	Northern reduced sediment	890	15.57
PC-MN2	1154	Methane-rich	Northern reduced sediment	1060	18.62
PC-MN3	1154	Methane-rich	Northern reduced sediment	1850	32.38
PC-MS1	1131	Methane-rich	Southern reduced sediment	2500	43.86

lular or intercellular bacterial symbionts that consumed methane and/or sulfide.[38,39] Throughout the three cruises, no significant changes were observed in the spatial distribution and variation of methane concentrations in the cold seep, and the dense chemosynthetic communities remained stable as well (Figure 1). *In situ* detection revealed the pattern of cold seep eruptions remained relatively stable on annual timescales, which could assist in developing a consistent geochemical model. Thus, we were able to evaluate the methane flux from the seabed into the hydrosphere of the cold seep.

Fate of methane from the active seep

The continental slope of the northern SCS is characterized by canyons and ridges.[40] Site F is located on the southern summit of the Formosa Ridge, which features steep flanks with a maximum slope angle exceeding 30°.[17] As a result, even minor changes in bottom currents could significantly affect the estimation of methane inputs. Based on our *in situ* observations, the bottom currents exhibited relatively high velocities, likely due to the complex location and topography of the seepage area. Microbiome metabolism in the water column and sediments of cold seep was essential for methane sequestration and biogeochemical cycling. A recent study revealed the heterogeneity in the composition and function of microorganisms in water column across the Site F.[41] Compared to the upper water layers, the bottom water hosted a unique chemoautotrophic community that derived energy from reducing compounds in seeping fluids. This process was primarily carried out by Methylococcales, which accounted for 9.06% of the total bacterial abundance in seeping fluids.[41] It possessed a complete methane oxidation pathway in their metagenome-assembled genomes (MAGs). The bottom water of the seepage was dominated by chemosynthetic microbes, such as methane-oxidizing bacteria (MOB) from Methylococcales and sulfur-oxidizing bacteria (SOB) from Thiotrichales and Campylobacterales. The anaerobic methane-oxidizing archaea (ANME) and sulfate-reducing bacteria (SRB) oxidized the methane into bicarbonate (HCO_3^-) through the anaerobic oxidation of methane (AOM) within the reduced sediments at the cold seep site F.[35] Metagenomic analyses linked to geochemistry showed that the coupling of multi-element cycles, specifically carbon, nitrogen, and sulfur, enhanced metabolic complementarity among the dominant microbes in the hydrosphere near an active cold seep vent.

In the cold seep, the methane oxidation rate measured in different areas can vary significantly across both space and time, as microbial activity is influenced by the presence of aerobic methanotrophs under varying ambient conditions.[42] The spatial heterogeneity of methane oxidation rate (MO_x) could have several impacts on the accuracy of the estimates and the associated uncertainty. Variations in oxidation rates across different regions can result in estimation errors, thereby affecting the precision of flux calculations. Moreover, spatial heterogeneity could amplify uncertainty in the estimates. Based on our *in situ* methane concentration measurements, we utilized a high methane oxidation (*MOx*) value alongside elevated methane concentrations to calculate the microbial contribution to methane consumption in the model.[29] To quantify the uncertainty related to the spatial heterogeneity of MO_x, we have employed a sensitivity analysis to assess the impact of varying methane oxidation rates on flux estimation. The variations in methane flux estimates resulting from changes in MO_x were illustrated in Figure 5B. Large quantities of methane can indeed be removed via aerobic methane oxidation within the water column at the active cold seeps. However, microbial methane oxidation was not the dominant methane removal mechanism at these sites, contrary to our initial assumptions. Our model results indicated that aerobic methanotrophs oxidized, on average, less than 10% of the methane emitted at seep sites (Figure 5A). This suggested that over 90% of the methane was likely transported and oxidized farther away from the seepage sites, ultimately contributing to the background methane levels in the surrounding seas. In its dissolved form, fluid advection and diffusion across

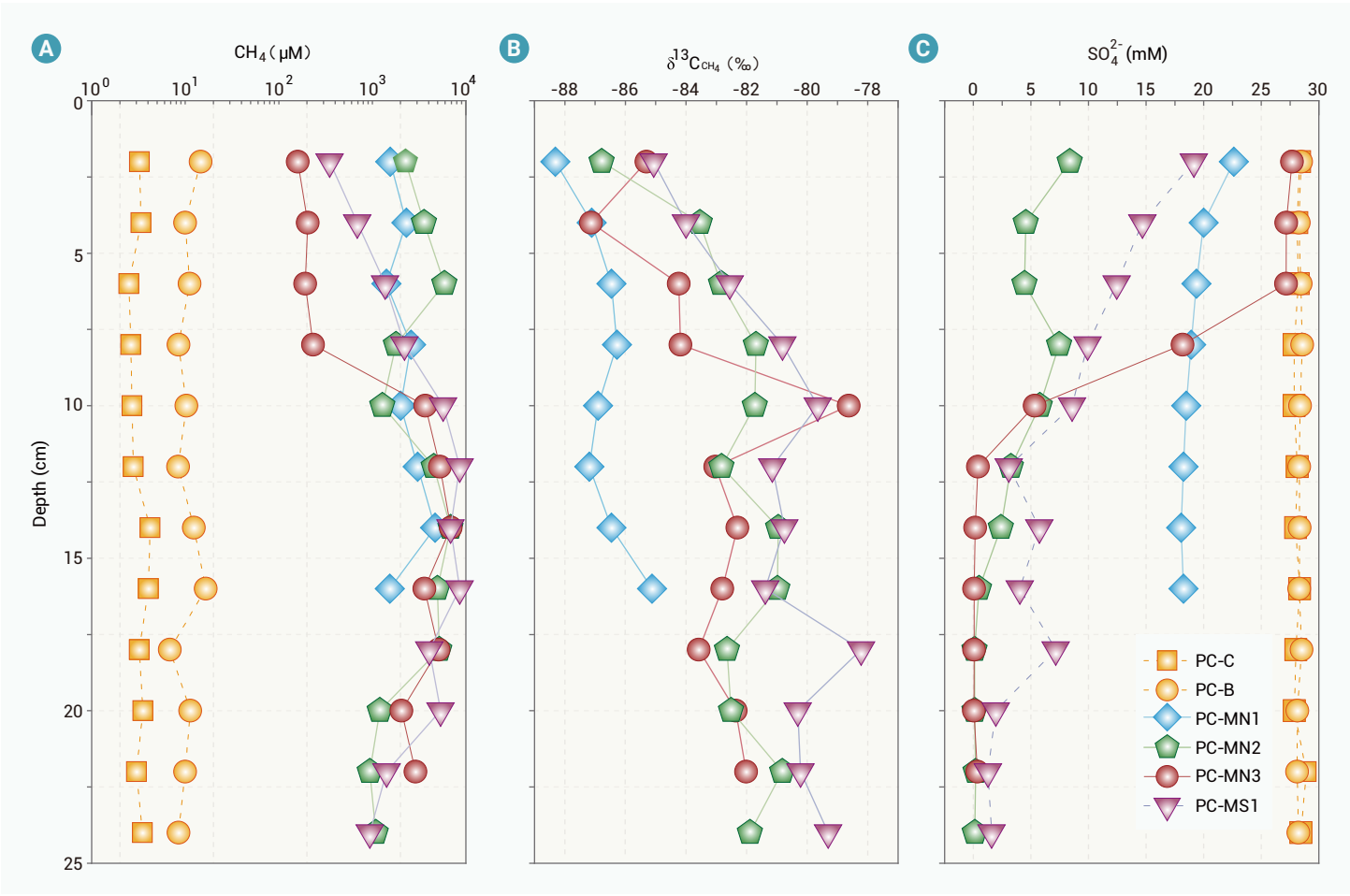

Figure 6. Depth concentration profiles of the methane, the carbon isotope of the methane and sulfate in the cold seep sediments (A) Vertical distribution of the methane concentration. (B) Vertical distribution of the carbon isotope of the methane. (C) Vertical distribution of the sulfate concentration.

concentration gradients resulted in the flux of methane toward the bottom waters over extensive areas of the seafloor. Due to the high velocity of currents and the low temperature of the bottom waters, venting methane may be carried to other water layers, where it could stabilize and undergo complete oxidation. Similarly, the investigation of dissolved methane in the water column above the Håkon Mosby Mud Volcano (HMMV) indicated that the decrease in methane concentration in the seawater was more likely due to dilution rather than consumption.[43] In conclusion, our model results demonstrated a mechanism through which most of the seep methane could be transported away from site F.

Methane flux of the cold seep site F and its environmental control

A schematic diagram illustrating methane flux across different habitats at cold seep site F was created (Figure 7). Although observed across large areas around the cold seep, the magnitude of dissolved methane flux from various sediment sites varied significantly over very small distances of the seafloor (Table 3). The magnitude of dissolved methane flux from methane-rich sediments at site F is comparable to that observed in methane-rich sediments at Cape Lookout Bight, where diffusive methane flux ranged from 1 to 3 mmol m^{-2} d^{-1},[44] but lower than that reported for sediments covered with bacterial mats located on Hydrate Ridge (30-100 mmol m^{-2} d^{-1}).[45,46] More importantly, the calculated methane flux from the active seep area, based on the model, was several orders of magnitude higher than that from the surrounding sediment area (Figure 7). Therefore, if we rely solely on the dissolved methane fluxes from the sediments into the overlying water to estimate methane emissions from the active cold seep, the values would be significantly underestimated.

In our study, the model utilized *in situ* measurements of methane concentration in the water column, methane oxidation rate, and bottom currents to estimate a significantly higher methane emission from seepage. All the incorporated chemical and physical parameters likely contributed to variations in emission estimates. Additional CH_4 oxidation that may occur outside of the studied region would further increase the emission estimate. The result is an estimate of dissolved methane that excludes the contribution of gas bubbles. For these reasons, we regard these emission estimates as lower bounds for the true emissions from the active seep. To facilitate comparison with published data from other cold seeps at varying water depths (Figure 8, Data S3), we also converted the methane emissions and flux to an annual basis.

The methane flux in our study area was significantly higher than that in previously investigated cold seeps. We propose that the discrepancies in methane flux estimates primarily arise from differences in methodology and variations in cold seep eruption dynamics. With advancements in deep-sea observation technologies, we have employed ROV equipped with high-definition cameras and *in situ* sensors, enabling more detailed exploration and investigation within visualized deep-sea environments. Furthermore, our study focused on the methane release in the active seepage center, where the bottom seawater contained high concentrations of methane. However, the methane emissions calculated here were relatively low. This is because the area of active seepage with dense communities only covered 1,500 m^2, as reported from comprehensive acoustic and visual data of site F.[23] If we assume that these methane flux values are representative of SCS continental margins with high seepage potential, we could extrapolate the methane flux estimates to the entire 358.1 km^2 area.[47] This would result in approximately 0.70-4.22 Gmol yr^{-1} of dissolved methane being released into the overlying hydrosphere of the SCS continental margins, excluding the methane flux at the sediment-water interface. Our research should be considered reliable as the relevant estimates are derived from *in situ* observations and models, which significantly reduce the uncertainty in the results. The regional methane fluxes in the SCS emphasize the importance of quantifying the dissolved methane flux from individual cold seeps to improve the global

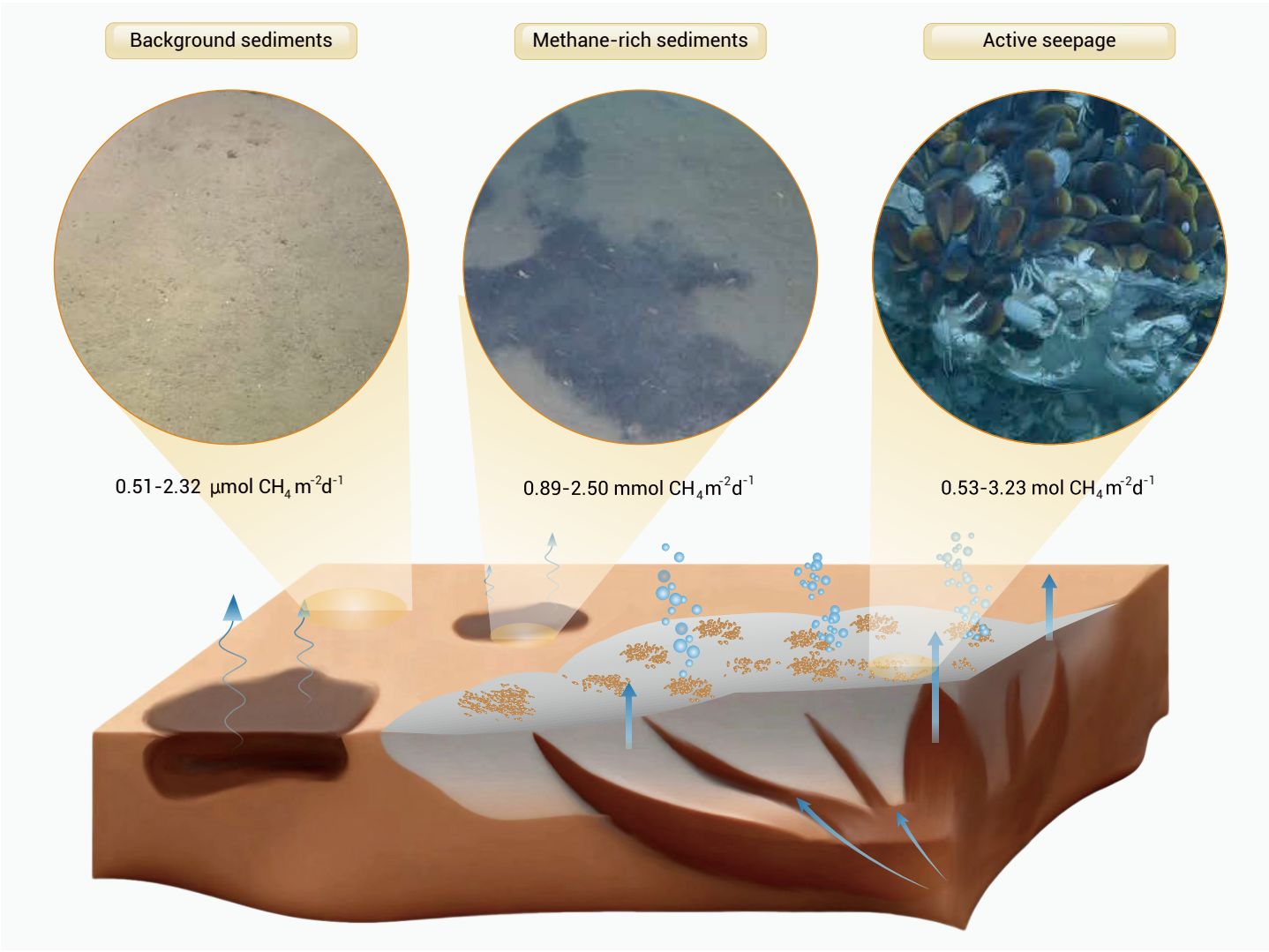

Figure 7. Methane flux at different habitats of the cold seep site F.

methane budget.

Although a significant amount of methane bypassed microbial oxidation in the native water above the seafloor where it was released, it would eventually undergo aerobic consumption in the water column farther away. Since the end product of aerobic CH_4 oxidation is CO_2 and the bottom current in this region is strong, the aerobic oxidation of CH_4 from this extensive CH_4 emission region could significantly affect the DIC chemistry of the adjacent seawater in the SCS. In the context of global warming, such phenomena could influence pH and lead to the release of CO_2 derived from CH_4 into the atmosphere. Therefore, continuous and widespread methane eruptions could significantly impact the surrounding seawater environment by altering seawater chemistry or enhancing the reproduction of microorganisms fueled by dissolved methane transported via advection or diffusion.

Methane budget to the ocean

As the methane flux estimated based on *in situ* observations in this study was significantly higher than that observed in previously investigated cold seeps, we attempted to extrapolate the total methane emission rates from individual seeps on the SCS continental slope to the broader area of global continental slopes. We assumed that active cold seep systems worldwide account for approximately 0.05% of the continental slope area,[48] and that the total seafloor area of global continental slopes is 3.01×10^7 km^2.[49] Active seeps worldwide could yield an estimated average of 126 Tg C annually as dissolved methane into the hydrosphere. This amount is roughly twice as high as the methane emissions from cold seeps along the global shallow continental shelves (8.0–65 Tg C).[50] Our estimation was higher than the methane released from mud volcanoes to ocean water in previous global estimates (1.1–20.3 Tg C).[2,51,52] Given the variability in activity and methane emission rates of cold seeps, it is important to note that the current extrapolation conclusions are primarily applicable to highly active cold seep systems with similar geological backgrounds. Despite uncertainties in methane flux calculations, the results obtained provide valuable insights that could enhance future methane budget estimates for individual geological structures and oceans. Future research could involve broader methane flux measurements across different geographical regions and cold seep sites to improve the applicability and accuracy of this extrapolation. This estimation represents a minimum of the total methane emissions, suggesting that the contribution of methane from deep-sea cold seeps to the global methane budget may be underestimated.

The dissolved methane emitted from active seepage into the overlying water fuels the marine ecosystem of the adjacent seawater. However, for oceanic methane budgets, dissolved methane effluxes were previously not considered. Given the significance of oceanic methane emissions and their spatial proximity to regions targeted for gas hydrate exploration, prioritizing active cold seep systems on the global continental slopes with the highest biomass for ecosystem monitoring and protection is crucial. Based on the data obtained during our study, it is evident that dissolved methane discharge significantly contributes to ocean methane budget and should not be overlooked.

CONCLUSION

In this study, the spatiotemporal variation of the seafloor environmental conditions at the cold seep site F was identified through *in situ* observations. These observations enhanced our understanding of the biogeochemical

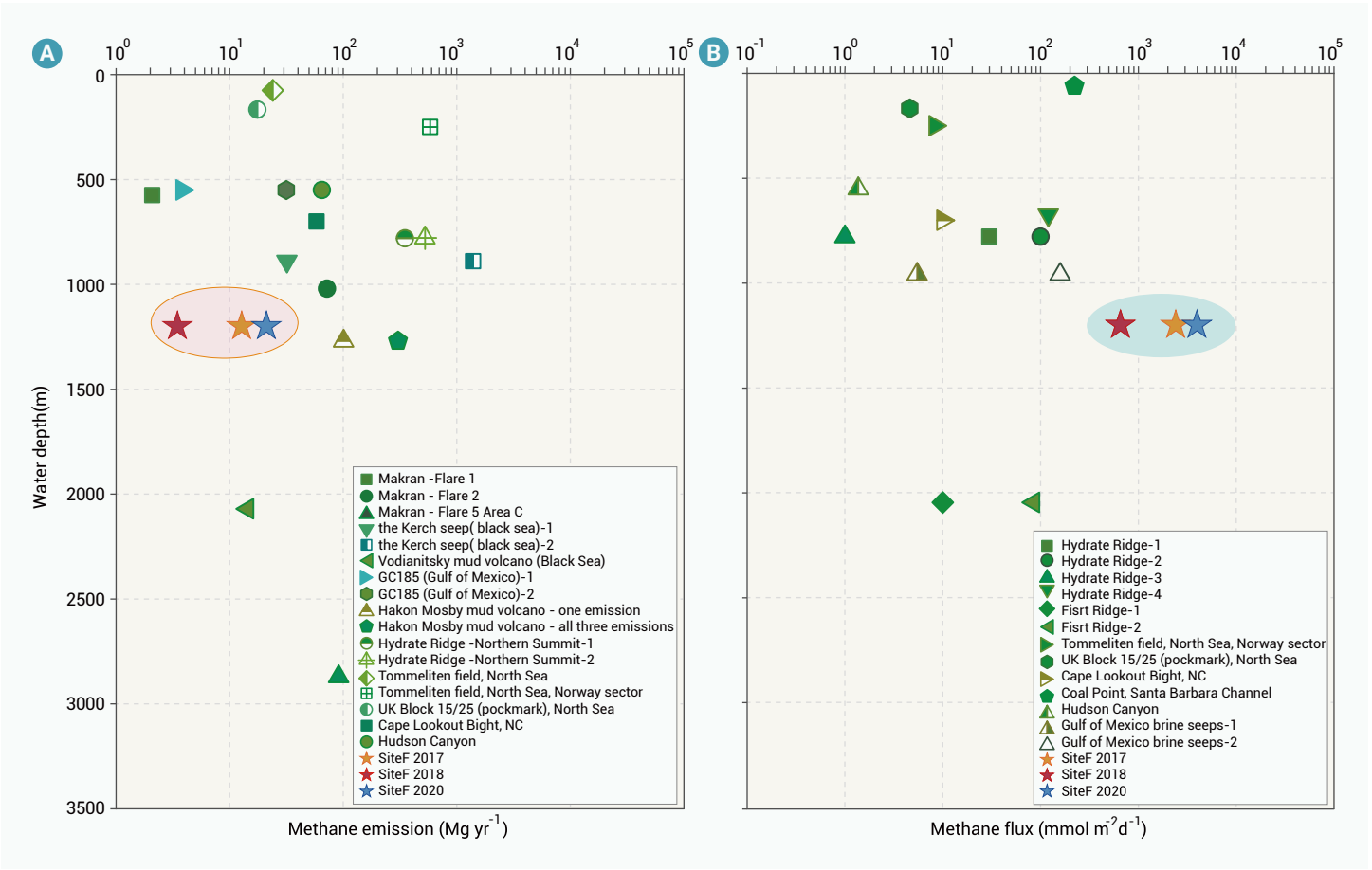

Figure 8. Comparison of methane emission and flux at site F with those from other cold seeps (A) Methane emission at site F with those from other cold seeps. (B) Methane flux at site F with those from other cold seeps.

processes occurring in the hydrosphere above site F and their connections to surrounding ecosystems. Results from a steady-state model over three years indicated that horizontal advection was likely the primary mechanism for the migration and removal of methane released into the hydrosphere, followed by vertical diffusion and microbial oxidation. The calculated methane flux in the active seep area, based on *in situ* measurements, was several orders of magnitude greater than the diffusive fluxes at the sediment-water interface. Consequently, methane emissions from the active cold seep would be significantly underestimated if evaluated solely based on the dissolved methane fluxes at the sediment-water interface. *In situ* observations are essential, and additional measurements of methane flux are needed to improve estimates of the oceanic methane budget.

Our study indicates that approximately 0.70-4.22 Gmol yr^{-1} of dissolved methane is released into the hydrosphere of the SCS continental margins. The regional methane flux in the SCS underscores the importance of dissolved methane flux from individual cold seeps in refining the global budget quantification of methane. Extrapolating the methane flux to the active seeps worldwide could yield approximately 126 Tg C liberated into the hydrosphere each year as the dissolved form of methane. The findings highlight deep-water active seeps as a significant source of methane to the ocean. Therefore, the dissolved methane flux from active seeps along the continental slope should be taken into account when evaluating oceanic methane budgets. This approach, combining *in situ* observations and modeling, could provide more precise insights into regional methane budget assessments and enhance our understanding of the oceanic methane budget.

REFERENCES

1. Suess E. (2014). Marine cold seeps and their manifestations: Geological control, biogeochemical criteria and environmental conditions. *Int. J. Earth. Sci.* **103**:1889–1916. DOI:10.1007/s00531-014-1010-0
2. Judd A. G. (2003). The global importance and context of methane escape from the seabed. *Geo-Mar. Lett.* **23**:147–154. DOI:10.1007/s00367-003-0136-z
3. Reeburgh W. S. (2007). Oceanic methane biogeochemistry. *Chem. Rev.* **107**:486–513. DOI:10.1021/cr050362v
4. Romer M., Sahling H., Pape T., et al. (2012). Quantification of gas bubble emissions from submarine hydrocarbon seeps at the Makran continental margin (offshore Pakistan). *J. Geophys. Res-Oceans.* **117**:1–19. DOI:10.1029/2011jc007424
5. de Beer D., Sauter E., Niemann H., et al. (2006). *In situ* fluxes and zonation of microbial activity in surface sediments of the Hakon Mosby Mud Volcano. *Limnol. Oceanogr.* **51**:1315–1331. DOI:10.4319/lo.2006.51.3.1315
6. Sommer S., Linke P., Pfannkuche O., et al. (2010). Benthic respiration in a seep habitat dominated by dense beds of ampharetid polychaetes at the Hikurangi Margin (New Zealand). *Mar. Geol.* **272**:223–232. DOI:10.1016/j.margeo.2009.06.003
7. Philip B. T., Denny A. R., Solomon E. A., et al. (2016). Time-series measurements of bubble plume variability and water column methane distribution above Southern Hydrate Ridge, Oregon. *Geochem. Geophy. Geosy.* **17**:1182–1196. DOI:10.1002/2016gc006250
8. Sahling H., Roemer M., Pape T., et al. (2014). Gas emissions at the continental margin west of Svalbard: Mapping, sampling, and quantification. *Biogeosciences.* **11**:6029–6046. DOI:10.5194/bg-11-6029-2014
9. Skarke A., Ruppel C., Kodis M. et al. (2014). Widespread methane leakage from the sea floor on the northern US Atlantic margin. *Nat. Geosci.* **7**:657–661. DOI:10.1038/ngeo2232
10. Weber T. C., Mayer L., Jerram K., et al. (2014). Acoustic estimates of methane gas flux from the seabed in a 6000 km^2 region in the Northern Gulf of Mexico. *Geochem. Geophys. Geosy.* **15**:1911–1925. DOI:10.1002/2014GC005271
11. Fischer D., Sahling H., Noethen K., et al. (2012). Interaction between hydrocarbon seepage, chemosynthetic communities, and bottom water redox at cold seeps of the Makran accretionary prism: Insights from habitat-specific pore water sampling and modeling. *Biogeosciences.* **9**:2013–2031. DOI:10.5194/bg-9-2013-2012
12. Bergquist D. C., Fleckenstein C., Szalai E. B., et al. (2004). Environment drives physiological variability in the cold seep mussel Bathymodiolus childressi. *Limnol. Oceanogr.* **49**:706–715. DOI:10.4319/lo.2004.49.3.0706
13. Du Z. F., Zhang X., Luan Z. D., et al. (2018). *In situ* raman quantitative detection of the cold seep vents and fluids in the chemosynthetic communities in the South China sea. *Geochem. Geophy. Geosy.* **19**:2049–2061. DOI:10.1029/2018gc007496
14. Lin S., Lim Y., Liu C. S., et al. (2007). Formosa Ridge, a cold seep with densely populated chemosynthetic community in the passive margin, southwest of Taiwan. *Geochim. Cosmochim. Ac.* **71**:A582–A582.

15. Zhao Y., Xu T., Law Y. S., et al. (2020). Ecological characterization of cold-seep epifauna in the South China sea. *Deep-Sea. Res. Pt I.* **163**:103361. DOI:10.1016/j.dsr.2020.103361
16. Kunath P., Crutchley G., Chi W.C., et al. (2022). Episodic venting of a submarine gas Seep on geological time scales: Formosa ridge, Northern South China sea. *J. Geophys. Res-Sol. Ea.* **127**:e2022JB024668. DOI:10.1029/2022jb024668
17. Berndt C., Crutchley G., Klaucke I., et al. (2014). Geological controls on the gas hydrate system of Formosa Ridge, South China sea. OCEANS 2014 - TAIPEI. pp:1-4. DOI:10.1109/OCEANS-TAIPEI.2014.6964481
18. Chuang P. C., Yang T. F., Hong W. L., et al. (2010). Estimation of methane flux offshore SW Taiwan and the influence of tectonics on gas hydrate accumulation. *Geofluids.* **10**:497–510. DOI:10.1111/j.1468-8123.2010.00313.x
19. Tong H., Feng D., Cheng H., et al. (2013). Authigenic carbonates from seeps on the northern continental slope of the South China Sea: New insights into fluid sources and geochronology. *Mar. Petrol. Geol.* **43**:260–271. DOI:10.1016/j.marpetgeo.2013.01.011
20. Han X., Suess E., Liebetrau V., et al. (2014). Past methane release events and environmental conditions at the upper continental slope of the South China sea: Constraints by seep carbonates. *Int. J. Earth. Sci.* **103**:1873–1887. DOI:10.1007/s00531-014-10185
21. Feng D. and Chen D. (2015). Authigenic carbonates from an active cold seep of the northern South China sea: New insights into fluid sources and past seepage activity. *Deep-Sea. Res. Pt II.* **122**:74–83. DOI:10.1016/j.dsr2.2015.02.003
22. Zhang X., Du Z. F., Luan Z. D., et al. (2017). *In Situ* Raman Detection of Gas Hydrates Exposed on the Seafloor of the South China sea. *Geochem. Geophy. Geosy.* **18**:3700–3713. DOI:10.1002/2017gc006987
23. Wang B., Du Z., Luan Z., et al. (2021). Seabed features associated with cold seep activity at the Formosa Ridge, South China sea: Integrated application of high-resolution acoustic data and photomosaic images. *Deep-Sea. Res. Pt I.* **177**:103622. DOI:10.1016/j.dsr.2021.103622
24. Guan H., Feng D., Wu N., et al. (2016). Methane seepage intensities traced by biomarker patterns in authigenic carbonates from the South China Sea. *Org. Geochem.* **91**:109–119. DOI:10.1016/j.orggeochem.2015.11.007
25. Liang Q., Hu Y., Feng D., et al. (2017). Authigenic carbonates from newly discovered active cold seeps on the northwestern slope of the South China Sea: Constraints on fluid sources, formation environments, and seepage dynamics. *Deep-Sea. Res. Pt I.* **124**:31–41. DOI:10.1016/j.dsr.2017.04.015
26. Graves C. A., Steinle L., Rehder G., et al. (2015). Fluxes and fate of dissolved methane released at the seafloor at the landward limit of the gas hydrate stability zone offshore western Svalbard. *J. Geophys. Res-Oceans.* **120**:6185–6201. DOI:10.1002/2015jc011084
27. Weinstein A., Navarrete L., Ruppel C., et al. (2016). Determining the flux of methane into Hudson Canyon at the edge of methane clathrate hydrate stability. *Geochem. Geophy. Geosy.* **17**:3882–3892. DOI:10.1002/2016gc006421
28. Yang Q., Zhao W., Liang X., et al. (2016). Three-dimensional distribution of turbulent mixing in the South China sea. *J. Phys. Oceanogr.* **46**:769–788. DOI:10.1175/jpo-d-14-0220.1
29. Mau S., Tu T.-H., Becker M., et al. (2020). Methane seeps and independent methane plumes in the South China sea offshore Taiwan. *Front. Mar. Sci.* **7**:543. DOI:10.3389/fmars.2020.00543
30. Boudreau B. P., Luo Y., Meysman F. J. R., et al. (2015). Gas hydrate dissociation prolongs acidification of the Anthropocene oceans. *Geophys. Res. Lett.* **42**:9337–9344. DOI:10.1002/2015gl065779
31. Iversen N. and Jorgensen B. B. (1993). Diffussion-coefficient of sulfate and methane in marine-sediments-influence of porosity. *Geochim. Cosmochim. Ac.* **57**:571–578. DOI:10.1016/0016-7037(93)90368-7
32. Paulmier A., Ruiz-Pino D. (2009). Oxygen minimum zones (OMZs) in the modern ocean. *Prog. Oceanogr.* **80**:113–128. DOI:10.1016/j.pocean.2008.08.001
33. Sommer S., Tuerk M., Kriwanek S., et al. (2008). Gas exchange system for extended *in situ* benthic chamber flux measurements under controlled oxygen conditions: First application-sea bed methane emission measurements at Captain Arutyunov mud volcano. *Limnol. Oceanogr-Meth.* **6**:23–33. DOI:10.4319/lom.2008.6.23
34. Ma J., Li X., Song J., et al. (2023). Relationship and stratification of multiple marine ecological indicators: A case study in the M2 seamount area of the Western Pacific Ocean. *Ecol. Indic.* **146**:109804. DOI:10.1016/j.ecolind.2022.109804
35. Sun Q.-l., Xu K., Cao L., et al. (2023). Nitrogen and sulfur cycling driven by Campylobacterota in the sediment-water interface of deep-sea cold seep: A case in the South China sea. *Mbio.* **14**:1–17. DOI:10.1128/mbio.00117-23
36. Levin L. A., Baco A. R., Bowden D. A., et al. (2016). Hydrothermal Vents and Methane Seeps: Rethinking the Sphere of Influence. *Front. Mar. Sci.* **3**:72. DOI:10.3389/fmars.2016.00072
37. Wang H., Wang X., Cao L.,et al. (2023). Macrofauna community of the cold seep area at Site F, South China Sea. *Front. Mar. Sci.* **10**:1068916. DOI:10.3389/fmars.2023.1068916
38. Sun Y., Wang M. X., Li L. L., et al. (2017). Molecular identification of methane monooxygenase and quantitative analysis of methanotrophic endosymbionts under laboratory maintenance in Bathymodiolus platifrons from the South China Sea. *Peerj.* **5**:e3565. DOI:10.7717/peerj.3565
39. Watsuji T. O., Yamamoto A., Takaki Y., et al. (2014). Diversity and methane oxidation of active epibiotic methanotrophs on live Shinkaia crosnieri. *Isme. J.* **8**:1020–1031. DOI:10.1038/ismej.2013.226
40. Berndt C., Chi W. C., Jegen M., et al. (2019). Tectonic controls on gas hydrate distribution off SW Taiwan. *J. Geophys. Res-Sol. Ea.* **124**:1164–1184. DOI:10.1029/2018jb016213
41. Liu Y., Zhang H., Cao L., et al. (2025). Methane filtration and metabolic cooperation of microbial communities in cold seep water columns from south china sea. *Commun. Biol.* **8**:1052. DOI:10.1038/s42003-025-08471-4
42. Steinle L., Graves C. A., Treude T., et al. (2015). Water column methanotrophy controlled by a rapid oceanographic switch. *Nat. Geosci.* **8**:378–382. DOI:10.1038/ngeo2420
43. Damm E. and Budéus G. (2003). Fate of vent-derived methane in seawater above the Hakon Mosby mud volcano (Norwegian Sea). *Mar. Chem.* **82**:1–11. DOI:10.1016/s0304-4203(03)00031-8
44. Martens C. S. and Valklump J. (1980). Biogeochemical cycling in an organic-rich coastal marine basin.1. Methane sediment-water exchange processes. *Geochim. Cosmochim. Ac.* **44**:471-490. DOI:10.1016/0016-7037(80)90045-9.
45. Torres M. E., McManus J., Hammond D. E., et al. (2002). Fluid and chemical fluxes in and out of sediments hosting methane hydrate deposits on Hydrate Ridge, OR, I: Hydrological provinces. *Earth. Planet. Sc. Lett.* **201**:525–540. DOI:10.1016/s0012-821x(02)00733-1
46. Tryon M. D., Brown K. M. and Torres M. E. (2002). Fluid and chemical flux in and out of sediments hosting methane hydrate deposits on Hydrate Ridge, OR, II: Hydrological processes. *Earth. Planet. Sc. Lett.* **201**:541–557. DOI:10.1016/s0012-821x(02)00732-x
47. Ke Z., Li R., Chen Y., et al. (2022). A preliminary study of macrofaunal communities and their carbon and nitrogen stable isotopes in the Haima cold seeps, South China Sea. *Deep-Sea. Res. Pt I.* **184**:103774. DOI:10.1016/j.dsr.2022.103774
48. Boetius A. and Wenzhofer F. (2013). Seafloor oxygen consumption fuelled by methane from cold seeps. *Nat. Geosci.* **6**:725–734. DOI:10.1038/Ngeo1926
49. Egger M., Riedinger N., Mogollon J. M., et al. (2018). Global diffusive fluxes of methane in marine sediments. *Nat. Geosci.* **11**:421–425. DOI:10.1038/s41561-018-0122-8
50. Hovland M., Judd A. G. and Burke R. A. (1993). The global flux of methane from shallow submarine sediments. *Chemosphere.* **26**:559–578. DOI:10.1016/0045-6535(93)90442-8
51. Milkov A. V., Sassen R., Apanasovich T. V., et al. (2003). Global gas flux from mud volcanoes: A significant source of fossil methane in the atmosphere and the ocean. *Geophys. Res. Lett.* **30**:1037. DOI:10.1029/2002gl016358
52. Felden J., Wenzhoefer F., Feseker T., et al. (2010). Transport and consumption of oxygen and methane in different habitats of the Hakon Mosby Mud Volcano (HMMV). *Limnol. Oceanogr.* **55**:2366–2380. DOI:10.4319/lo.2010.55.6.2366

FUNDING AND ACKNOWLEDGMENTS

This work was financially supported by the National Natural Science Foundation of China (Grant No. 42030407), the Science & Technology Fundamental Resources Investigation Program (Grant No. 2024FY101000), Marine S&T Fund of Shandong Province for Pilot National Laboratory for Marine Science and Technology (Qingdao) (Grant No. 22QNLM030004), the NSFC Innovative Group Grant (Grant No. 42221005), the National Natural Science Foundation of China (Grant No. 42176048), and the Strategic Priority Research Program of the Chinese Academy of Sciences (Grant No. XDB42020401). The authors are grateful to the captain and crews of the R/V Kexue, as well as the ROV Faxian operating teams, for their assistance with in situ investigation and sample collections. The funders had no role in study design, data collection and analysis, decision to publish, or preparation of the manuscript.

AUTHOR CONTRIBUTIONS

L.C., W.M.X., and L.C.L. conceptualized the research. L.C., C. L., H. Z. and H.W. performed the *in situ* measurement and collected the samples. L.C., W.M.X., C.L., X.B.R. and L.C.L analyzed the results and wrote the first draft of the article. L. Z., H. C. and Z.Z.S. contributed substantially to revisions. All authors contributed to the manuscript and approved the final version.

DECLARATION OF INTERESTS

The authors declare no competing interests.

DATA AND CODE AVAILABILITY

Research data associated with this article are presented in the paper and/or the supplementary materials. Data are also available from the corresponding author upon reasonable request.

LEAD CONTACT WEBSITE

Chaolun Li https://www.researchgate.net/profile/Chaolun-Li
Minxiao Wang https://www.researchgate.net/profile/Minxiao-Wang